Available online at www.sciencedirect.com
SCIENCE DIRECT®
Diamond and Related Materials 12 (2003) 2178–2185
DIAMOND AND RELATED MATERIALS
www.elsevier.com/locate/diamond

Simulation of H–C–S containing gas mixtures relevant to diamond chemical vapour deposition

J.R. Petherbridge, P.W. May*, D.E. Shallcross, J.N. Harvey, G.M. Fuge, K.N. Rosser, M.N.R. Ashfold

School of Chemistry, University of Bristol, Cantocks Close, Bristol BS8 1TS, UK

Received 17 June 2003; received in revised form 29 July 2003; accepted 29 July 2003

Abstract

Mole fractions of 24 species present within $x\%H_2S/1\%CH_4/H_2$ ($x=0$–1%) and $1\%CS_2/H_2$ gas mixtures have been calculated using the CHEMKIN computer package in conjunction with a mechanism based on the composite conversion: $CH_4 + 2H_2S \rightleftharpoons CS_2 + 4H_2$. Arrhenius parameters for each elementary reaction involving S-containing species are presented, along with associated thermodynamic properties for each species. Molecular beam mass spectrometric measurements of species mole fractions in microwave activated $x\%H_2S/1\%CH_4/H_2$ ($x=0$–1%) mixtures agree well with the model calculations, if we assume a (reasonable) gas temperature of 1630 K. The agreement between similar measurements of both $0.5\%H_2S/1\%CH_4/H_2$ and $1\%CS_2/H_2$ hot filament activated gas mixtures is less good, but the calculations succeed in reproducing many of the observed trends in species mole fraction with change in filament temperature.

Keywords: Chemical vapour deposition; Sulfur doping; Gas phase modelling

1. Introduction

The many extreme physical and mechanical properties [1,2] of thin diamond films grown by chemical vapour deposition (CVD) have prompted interest in such films for use in electronic devices. CVD diamond films exhibiting p-type semiconductor properties are routinely grown by addition of B-containing gases to the standard CVD gas mixture ($1\%CH_4/H_2$) [3,4]. Such films find use as electrodes for harsh electrochemical applications (e.g. highly acidic solutions) [5] and in UV detectors [6]. However, obtaining n-type semiconducting diamond films by CVD has proved more challenging, mainly due to the fact that potential donor atoms (e.g. N, P, O and As) are larger than carbon, discouraging incorporation into the diamond lattice. However, n-type conductivity, as demonstrated by Hall effect measurements, has been reported following sulfur ion implantation into CVD homoepitaxial diamond (100) films [7]. Furthermore, Sakaguchi et al. [8–10] have reported that H_2S addition to a 1% CH_4/H_2 gas mixture during microwave plasma enhanced CVD leads to growth of semiconducting, homoepitaxial diamond films exhibiting n-type behaviour. Small H_2S additions (approx. 100 ppm) were found to improve crystallinity, though this trend was reversed upon further increases in H_2S concentration. Film growth rate was also observed to decline with increased H_2S addition, though the quality of the films (as assessed via Raman spectroscopy) was found to be relatively insensitive to changes in H_2S addition. Relatively, high Hall mobilities (597 $cm^2\ V^{-1}\ s^{-1}$) were measured [8] for films produced using H_2S doping levels of 50–100 ppm. However, a later report by Kalish et al. [11] showed that these samples were possibly polluted by boron and that the measured n-semiconductivity was caused by this combination. This idea was taken further by Eaton et al. [12] who showed that deliberately co-doping with B and S could make n-type diamond, so long as the ratio of B:S was within a very narrow range. However, recently Nakazawa et al. [13] reported that n-type diamond could be deposited without the need for B incorporation, and deduced that n-type conductivity

*Corresponding author. Tel.: +44-0-117-9289927; fax: +44-0-117-9251295.
E-mail address: paul.may@bris.ac.uk (P.W. May).

0925-9635/03/$ - see front matter © 2003 Elsevier B.V. All rights reserved.
doi:10.1016/S0925-9635(03)00294-2

of sulfur-doped diamond was caused by a sulfur-related mechanism.

Experimental measurements of gas phase species concentrations present during the growth of sulfur doped CVD diamond films from H_2S have been reported by both our group [14,15] and others [16]. In the work of Sternschulte et al. [16], gas was sampled via a glass capillary tube at a point downstream from the microwave (MW) plasma, and analysed using a quadrupole mass spectrometer. H_2S addition to a $1\%CH_4/H_2$ MW plasma was shown to cause a decrease in CH_3 concentrations, leading to a decrease in diamond film growth rate; these workers concluded that CH_4 and H_2S were reacting in the gas phase to form CS. We employed molecular beam mass spectrometry (MBMS), thereby sampling gas directly from the plasma and with less perturbation from gas-surface reactions. The technique has been used previously to obtain mole fractions of gas phase species present in a variety of gas mixtures, with and without dopant gas additions, using both hot filament [17,18] and MW [19,20] activation. Our measurements of $x\%H_2S/1\%CH_4/H_2$ MW plasmas yielded results in good accord with those of Sternschulte et al. [16] and led to a proposed mechanism, based on the overall Reaction (1), for the coupling of gas phase C and S containing species to form CS radicals and CS_2. The proposal was supported by simple thermodynamic arguments and on relative abundance grounds, CS was suggested as a possible carrier involved in S incorporation within the diamond lattice [15].

$$CH_4 + 2H_2S \underset{k_{-1}}{\overset{k_1}{\rightleftharpoons}} CS_2 + 4H_2 \qquad \text{(Reaction1)}$$

Barber and Yarbrough have reported computer simulations of the gas phase chemistry of activated H/C/S mixtures [21]. They concluded that addition of CS_2 to the $1\%CH_4/H_2$ mixture caused a reduction in the concentration of gas phase hydrocarbons, which, when considered in association with the rest of their proposed mechanism, accounted for the reduction in diamond film growth rates observed experimentally. Dandy [22] subsequently presented equilibrium calculations for $H_2S/CH_4/H_2$ gas mixtures and concluded that sulfur incorporation into the diamond lattice in such systems was most likely via the SH radical. More recently, Habner and Sommer [23] performed thermodynamic calculations for a hot filament reactor, which suggested that the CS formation increased the carbon transport to the film surface and that this might be responsible for an increase in film growth rate as S is added to the gas mixture.

However, all of these previous studies were confined to equilibrium thermodynamic calculations, with the kinetics relevant to a CVD environment neglected. Here, we present the results of kinetics calculations employing our S–C coupling mechanism and explore their relation to previously published experimental MBMS measurements of species mole fractions, with the aim of validating the proposed scheme. The simulations were carried out using the SENKIN code, which has been used in previous investigations of the gas phase chemistry leading to CVD diamond growth from C/H/O containing gas mixtures [19,20,24].

2. Simulations

The gas phase reactions occurring in a representative gas phase environment used for diamond CVD were simulated using the SENKIN code, which is part of the CHEMKIN package [25]. Reactions and temperature dependent rate constants for all C and H containing species involved in these calculations were obtained from the GRI-Mech 3.0 reaction mechanism database [26]. Data for reactions involving S containing species was obtained from the literature, with rate data for analogous O containing species reactions used when none for S were available. These reactions are labelled (*) in Table 1.

The sulfur species reactions and their temperature dependent rate constants used in the present work are presented in Table 1. In this scheme, reaction is initiated by breakdown of H_2S, both thermally and also via hydrogen abstraction, to form SH radicals (Reaction (1) and Reaction 2). CH_3 radicals (produced from CH_4 via analogous H abstraction reactions) combine with SH to form either CH_3SH or CH_2S (Reactions 3 and 4), which then undergo successive H-abstraction reactions (Reactions 5–9) to form CS and finally, CS_2 (via Reaction 10). Additional reactions form S (from SH, Reactions 11–13) and S_2 (Reactions 14–16). The kinetic data are presented here in the form of Arrhenius equation parameters, which allow calculation of the rate constant of the forward reaction, k_1 (as each is written) via Equation 1.

$$k_1 = A\ T^{\beta} \exp(-E_a/RT) \qquad (1)$$

The thermodynamic properties (e.g. standard heat capacity C_p, entropy S and enthalpy H, as functions of temperature) required by the package to calculate the reverse rate constant, k_{-1}, were obtained from the 'thermo30.dat' database [26]. Since detailed thermodynamic and kinetic data for some of the S containing species of current interest are not available in the literature, nor in the database, we have used the Gaussian 98 computational chemistry program [27] to generate minimised geometries for CH_3SH, CH_3S, CH_2S and HCS. These were then used to calculate the required enthalpy and Gibbs free energy corrections (with both calculations using the MP2/6-311G** basis set). The data for each species were then scaled to the values at

Table 1
Reaction scheme proposed for C–S coupling within C/H/S gas mixtures present in HF and MW diamond CVD reactors operating at ~20 Torr. Arrhenius parameters (see Eq. (1) for definitions) for each reaction are presented in units acceptable to the CHEMKIN package. Literature references for these kinetic data are also listed

Number	Reaction	A /(cm^3 mol^{-1} s^{-1})	β	E_a /(cal mol^{-1})	Reference
1	$H_2S \rightleftharpoons SH + H$	7.632×10^{14}	0.00	82155.00	[32]
2	$H_2S + H \rightleftharpoons SH + H_2$	1.078×10^{13}	0.00	2969.67	[32]
3	$SH + CH_3 \rightleftharpoons CH_3SH$	9.998×10^{12}	0.00	0.00	[33]
4	$SH + CH_3 \rightleftharpoons H_2 + CH_2S$	1.018×10^{12}	0.00	0.00	[34]*
5	$H + CH_3SH \rightleftharpoons CH_3 + H_2S$	6.926×10^{12}	0.00	1664.00	[35]
6	$H + CH_3SH \rightleftharpoons CH_3S + H_2$	2.903×10^{13}	0.00	2593.00	[35]
7	$H + CH_3S \rightleftharpoons CH_2S + H_2$	1.988×10^{13}	0.00	0.00	[36]*
8	$H + CH_2S \rightleftharpoons HCS + H_2$	5.252×10^{12}	1.77	2989.29	[36]*
9	$H + HCS \rightleftharpoons H_2 + CS$	1.211×10^{14}	0.00	0.00	[36]*
10	$SH + CS \rightleftharpoons H + CS_2$	3.232×10^{10}	1.50	495.00	[37]*
11	$H + SH \rightleftharpoons H_2 + S$	1.301×10^{13}	0.00	0.00	[38]
12	$CH_4 + S \rightleftharpoons CH_3 + SH$	2.042×10^{14}	0.00	19796.00	[39]
13	$H_2S + S \rightleftharpoons 2SH$	5.704×10^{14}	0.00	15045.00	[40]
14	$2S + M \rightleftharpoons S_2 + M$	1.200×10^{17}	−1.00	0.00	[26]*
15	$SH + S \rightleftharpoons S_2 + H$	2.409×10^{13}	0.00	0.00	[41]
16	$2SH \rightleftharpoons H_2 + S_2$	3.012×10^{10}	0.00	0.00	[41]

* Data for analogous C/H/O reaction used.

298 K, using calculation of ΔG_{reac} and ΔH_{reac} for a number of isodesmic reactions (i.e. same number of bonds present on either side of the reaction) involving CH_3SH, CH_3S, CH_2S and HCS.

An example follows for the calculation of H (at 298 K) for HCS. Firstly, ΔH_{reac} was obtained for the reaction of CS and H_2 forming HCS and H, by summing the change between products and reactants of the electronic energy and the enthalpy energy correction (using CCSD(T)/cc-pVDZ and MP2/6-311G** electronic structure calculations, respectively). The standard enthalpy $H°$, for HCS was then obtained via Hess's law type calculation, using literature values [28] of H for CS, H_2 and atomic H. The free energy, G for HCS was

Table 2
Thermodynamic data for CH_3SH, CH_3S, CH_2S and HCS, in the form of polynomial fits to $C_p°/R$, $H°/RT$, and $S°/R$ as functions of temperature (over two ranges, 298–1000 K and 1000–5000 K). The coefficients are defined in Eqs. (2)–(4). Calculated values of entropy and enthalpy at 298 K are also presented with H_{298K} data being compared with literature data

Temperature range/K	Coefficient	CH_3SH	CH_3S	CH_2S	HCS
298–1000	a_1	1.8873	1.5421	2.4953	3.5537
	a_2	1.5460×10^{-2}	1.5180×10^{-2}	6.1100×10^{-3}	2.0700×10^{-3}
	a_3	-5.6022×10^{-6}	1.0000×10^{-5}	4.3754×10^{-6}	2.4041×10^{-6}
	a_4	-1.8247×10^{-9}	3.8581×10^{-9}	-9.6164×10^{-9}	-3.7711×10^{-9}
	a_5	1.5779×10^{-12}	-4.0429×10^{-13}	4.2503×10^{-12}	1.4823×10^{-12}
	a_6	-3.9260×10^{3}	1.3532×10^{-4}	1.1906×10^{4}	3.5321×10^{4}
	a_7	1.5501×10^{1}	1.6659×10^{1}	1.1629×10^{1}	7.4244
1000–5000	a_1	4.5472	3.6110	3.4681	3.7778
	a_2	1.0180×10^{-2}	8.9200×10^{-3}	6.2500×10^{-3}	2.8700×10^{-3}
	a_3	-3.7614×10^{-6}	-3.6176×10^{-6}	-2.5499×10^{-6}	-1.0604×10^{-6}
	a_4	6.3502×10^{-10}	6.8596×10^{-10}	4.8585×10^{-10}	1.7918×10^{-10}
	a_5	-4.0058×10^{-14}	-4.9459×10^{-14}	-3.5164×10^{-14}	-1.1311×10^{-14}
	a_6	-4.8540×10^{3}	1.2974×10^{4}	1.1504×10^{4}	3.5163×10^{4}
	a_7	8.9853×10^{-1}	6.4563	5.9022	5.7494
H_{298K}/ (kJ mol^{-1})	Calculated	−22.69	121.21	107.60	303.34
	Experiment	−22.86[1]	121.00[2]	118.86[3]	301.14[3]
S_{298K}/(J mol^{-1} K^{-1})	255.83	244.42	231.27	235.01	

[1] Ref. [42].
[2] Derived using H_{298K} for CH_3SH from Ref. [42] along with the experimentally determined bond dissociation enthalpy of CH_3S–H (Ref. [43]) and H_{298K} of atomic H (Ref. [28]).
[3] Ref. [44].

calculated similarly, thereby allowing derivation of a value for the entropies *S*. Similar calculations allowed the determination of *H* and *S* at 298 K, for CH_3SH, CH_3S, CH_2S and HCS (as presented in Table 2). Thus, data for standard heat capacity, enthalpy and entropy (as functions of temperature) were estimated for the four species, in the form of polynomial fits to C_p°/R, H°/RT, and S°/R as functions of temperature. There are seven coefficients for each of two temperature ranges (298–1000 K and 1000–5000 K), which are defined in Eqs. (2)–(4).

$$\frac{C_p^o}{R} = a_1 + a_2T + a_3T^2 + a_4T^3 + a_5T^4 \quad (2)$$

$$\frac{H^o}{RT} = a_1 + \frac{a_2}{2}T + \frac{a_3}{3}T^2 + \frac{a_4}{4}T^3 + \frac{a_5}{5}T^4 + \frac{a_6}{T} \quad (3)$$

$$\frac{S^o}{R} = a_1\ln T + a_2T + \frac{a_3}{2}T^2 + \frac{a_4}{3}T^3 + \frac{a_5}{4}T^4 + a_7 \quad (4)$$

Values for these coefficients used in the present work are listed in Table 2.

Equilibrium mole fractions of the 24 transient and stable gas phase species involved in this reaction scheme were calculated for a chosen input gas mixture (e.g. 1% H_2S/1% CH_4/H_2) and fixed gas temperature, T_{gas} and pressure (20 Torr). As always with such zero dimensional (0-D) modelling, it is important to recognise the limitations of such an approach. The assumption of a single T_{gas} for all reactions in a given simulation is obviously a serious approximation, particularly in the case of hot filament (HF) activated gas mixtures that necessarily involve large temperature gradients [29]. The T_{gas} value chosen when simulating the MW activated gas mixtures (approx. 1630 K) is considered reasonable for a 1%CH_4/H_2 plasma in a low power (< 3 kW) reactor operating at ~40 Torr [19,29,30] and the region sampled in our MBMS measurements. No electron impact dissociation, ionic reactions or surface chemistry were included in the modelling; reaction is thus initiated solely by thermal dissociation. Finally, no transport into or out of the reaction volume is allowed in the zero-dimensional model. To mimic experiment, therefore, it is necessary to run the simulation for a finite (user selected) time *t*, here chosen to be 5 s, as found to be appropriate in our previous modelling of microwave activated H/C/O gas mixtures [19,20,24]. Under these conditions, the mixtures are still far from fully equilibrated. For example, the C_2H_2 'product' in a 1%H_2S/1%CH_4/98%H_2 gas mixture activated under the above conditions has only reached approximately 30% of its asymptotic mole fraction value at long time (t = 200 s). Calculations were run repeatedly in order to obtain species mole fraction plots as functions of gas mixture or gas temperature.

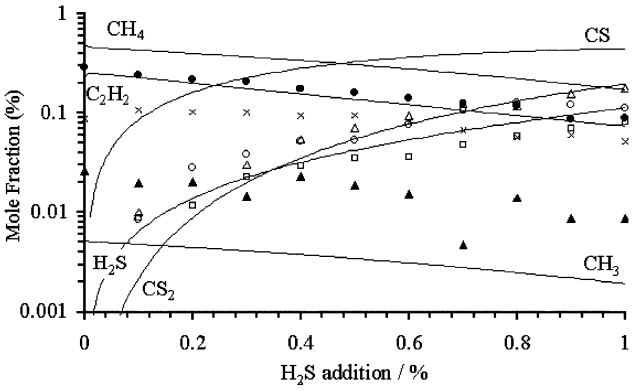

Fig. 1. Plot of species mole fraction (%) vs. H_2S addition to a 1%CH_4/H_2 gas mixture for both MBMS measurements from a microwave plasma (adapted from Ref. [14]) and SENKIN calculations that assume a reaction time of 5 s and T_{gas} = 1630 K. Conditions: Pressure 20 Torr. Key: SENKIN calculated mole fractions (%, solid lines, as labelled), experimental MBMS mole fractions (%), scaled to maintain a constant carbon mass balance (●) CH_4, (×) C_2H_2, (▲) CH_3, (□) H_2S, (△) CS_2 (○) CS.

3. Results and discussion

Fig. 1 shows a plot of species mole fraction (as a percentage of the total gas mixture) against H_2S addition for both MBMS measurements of a MW activated x%H_2S/1%CH_4/H_2 mixture and the corresponding SENKIN calculations at a fixed T_{gas} = 1630 K. Experimentally, the measured carbon mass balance was observed to fall with increasing H_2S addition (as shown in Fig. 5b of Ref. [14]). To aid comparison with the zero-dimensional model outputs, therefore, the mole fractions of the various C containing species measured by MBMS have been rescaled, so as to maintain a constant total carbon mass balance. Reassuringly, this has the effect of achieving S-balance across the full range of H_2S additions also. As Fig. 1 shows, the relative concentrations of the various hydrocarbon species and their variation with added H_2S are reproduced well by SENKIN, with CH_4, C_2H_2 and CH_3 mole fractions all falling as %H_2S is increased. Relative to the experimental measurements, the calculated mole fraction of the methyl radical, [CH_3], appears to be consistently underestimated by the calculations, whereas [CH_4] and [C_2H_2] are both overestimated. The general trends in [CS_2] and [H_2S] are also reproduced well by SENKIN, with both species mole fractions rising with increased H_2S addition. Discrepancies between calculation and experiment should not be surprising and can have several sources. Firstly, of course, there is the simplicity of the zero-dimensional model employed. The experiment samples a dynamic three-dimensional system involving many processes (e.g. transport of species between areas with varying gas temperatures) that are not included in the SENKIN model. Secondly, there are

real uncertainties in calibrating MBMS measurements of species concentrations; these we estimate to be ~25% for stable species like CH_4 and C_2H_2, but can be very much larger for radical species such as CH_3. Taking these limitations into account, the level of agreement achieved between experiment and simulation is quite remarkable.

The CS radical mole fraction predicted by the SENKIN calculations is almost an order of magnitude larger than the MBMS results. This discrepancy may reflect an error in the calibration factor we use to convert raw $m/z=44$ (CS) counts measured with the MBMS into mole fractions. Derivation of this factor requires some estimation of the partitioning between background $m/z=44$ signal within the mass spectrometer and that arising from within the molecular beam of gas sampled from the plasma—which we here assumed to be the same as determined previously in MBMS measurements of CH_3 radical mole fractions [17]. The difference between measurement and simulation may indicate that we are underestimating [CS] experimentally, which would also explain the apparent drop in carbon balance observed upon increasing H_2S additions. Additionally, we note that the main proposed loss mechanism for CS is reaction with HS (to form H and CS_2, Reaction 10 in Table 1), which we have modelled assuming kinetic data for the analogous reaction between HO and CO. If the loss rate of CS is actually faster, then the SENKIN calculations will overestimate [CS]. We reiterate, however, that the *trend* in measured [CS] with increasing H_2S addition is reproduced well by simulation.

Fig. 2a shows plots of experimental MBMS species mole fractions (as a percentage) for a $0.5\%H_2S/1\%CH_4/H_2$ gas mixture measured in a HF reactor at a distance of 5 mm from the filament, presented as a function of filament temperature, T_{fil}. Again, the data have been rescaled relative to that reported in Ref. [14], so as to maintain a constant carbon balance and to aid comparison with the model output. Again, this rescaling has the effect of achieving approximate S balance across the T_{fil} range also. SENKIN simulations for the same gas mixture, as a function of T_{gas}, are presented in Fig. 2b. The gas temperature falls rapidly with increasing distance from the hot filament and will typically be ~1000 K lower than T_{fil} at the point at which MBMS sampling occurs (5 mm distant from the HF) [29]. The constant T_{gas} assumption is thus more questionable when modelling HF activated gas mixtures. To aid (qualitative) comparison between experimental MBMS measurements and the SENKIN calculations of species mole fractions, we have offset the temperature scales in Fig. 2. Considering the inherent simplifications, the level of agreement between experiment and simulation is generally good. Mole fractions of both CH_4 and H_2S are predicted (and observed) to reduce with increased temperature, while $[CS_2]$ and $[C_2H_2]$ both rise. It should also be noted, however, that the simulations also predict CS to be present at detectable concentrations, but none was detected experimentally.

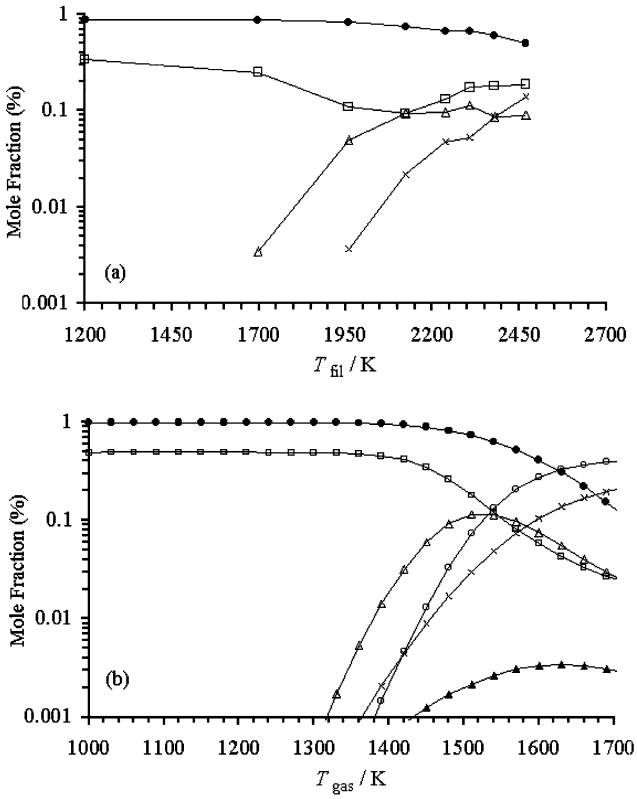

Fig. 2. Plots of (a) MBMS experimental species mole fractions (%) vs. T_{fil} for a HF activated gas mixture with gas sampled from a position 5 mm from the filament (scaled from Ref. [14] so as to maintain a constant carbon mass balance) and (b) SENKIN calculated mole fraction (%) vs. T_{gas} for a reaction time $t=5$ s. Conditions: pressure 20 Torr, gas mixture $0.5\%\ H_2S/1\%CH_4/H_2$. Key: (●) CH_4, (×) C_2H_2, (▲) CH_3, (□) H_2S, (△) CS_2 (○) CS.

Fig. 3 illustrates the qualitative agreement between measured (Fig. 3a) and simulated (Fig. 3b) species mole fractions (again plotted on a percentage scale) in the case of an HF activated $1\%CS_2/H_2$ gas mixture also with CS_2 breaking down as the T_{fil} is increased and undergoing reaction to form CH_4, H_2S and C_2H_2. As in the case of HF activated $H_2S/CH_4/H_2$ gas mixtures (Fig. 2), the raw data have been rescaled to compensate for the drop in the total carbon balance with increasing T_{fil} (and thus T_{gas}) that is observed experimentally. In HF activated gas mixtures this is generally attributed to the Soret effect, whereby the temperature gradient induces preferential diffusion of heavier components of a gas mixture (e.g. CS_2) away from the higher temperature filament/sampling orifice region [17]. There is one obvious discrepancy between the data sets: no CS was detected experimentally, although, the SENKIN calculations predict that it should be present in measurable concentrations. In both cases, we suspect this to reflect

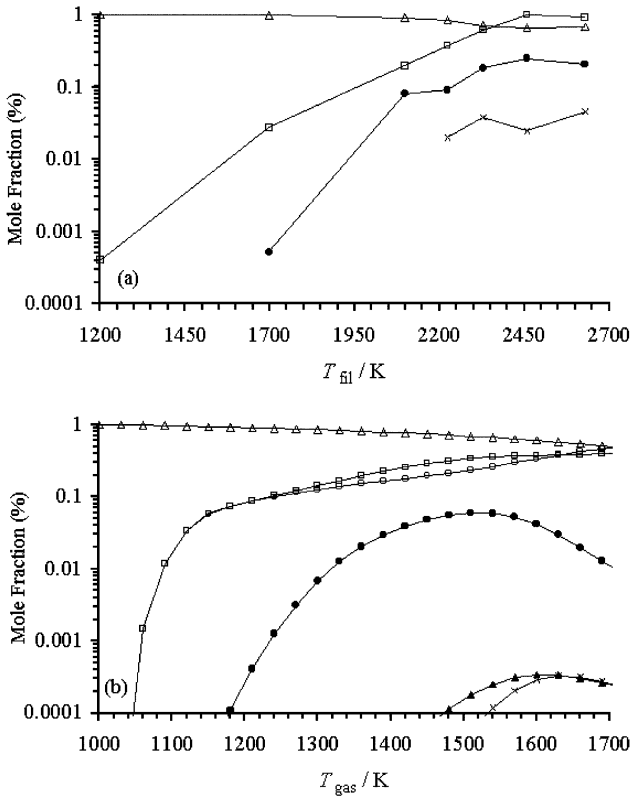

Fig. 3. Plots of (a) MBMS experimental species mole fractions (%) vs. T_{fil} for a HF activated gas mixture with gas sampled from a position 5 mm from the filament (scaled from Ref. [14] so as to maintain a constant carbon mass balance) and (b) SENKIN calculated mole fraction (%) vs. T_{gas} for a reaction time $t=5$ s. Conditions: pressure 20 Torr, gas mixture 1% CS_2/H_2. Key: (●) CH_4, (×) C_2H_2, (▲) CH_3, (□) H_2S, (△) CS_2 (○) CS.

primarily, the large temperature gradients present in the HF reactor, possibly compounded by any inadequacies in the temperature dependence of the CS chemistry used in the simulations.

All three sets of SENKIN calculations predict mole fractions for S and S_2 of $\sim 10^{-4}$%. This is an order of magnitude below the detection limit of the MBMS apparatus and is thus consistent with our non-observation of either of these species [14,15]. The SH radical has been proposed [22] as a possible carrier by which S is incorporated into a growing diamond lattice. No MBMS signals attributable to this species could be detected, in either the MW or HF activated gas mixtures. Consistent with this, the SENKIN simulations of a $1\%H_2S/1\%CH_4/H_2$ gas mixture under conditions equivalent to those used in Fig. 1b predict [SH] $\sim 10^{-4}$%, some 20× less than the predicted [CS], irrespective of the chosen integration time, *t*. This [CS]/[SH] ratio accords well with that determined in previous equilibrium thermodynamic calculations of $H_2S/CH_4/H_2$ gas mixtures at similar T_{gas} values [22].

The relative abundance of CS radicals in MW activated $H_2S/CH_4/H_2$ gas mixtures has led to suggestions that S incorporation into diamond films might occur via this species [14,15]. Such speculation gains support from the observations of significant S incorporation into CVD diamond films grown from MW activated gas mixtures, whereas films grown from HF activated mixtures contain at most trace S. These differences were rationalised, as here, by recognising the very difference volumes of gas exposed to the high temperatures necessary to facilitate coupling of C and S containing species [14]. If we proceed with the assumptions that (a) the diamond growth species is the methyl radical, as is now generally assumed in all other low power, H_2 rich CVD environments [31]; and (b) CS facilitates S incorporation into diamond films, then it has been suggested that the product $[CH_3]\times[CS]$ might provide some measure of optimal growth conditions for S-doped diamond films. In the case of SENKIN calculations for $xH_2S/1\%CH_4/H_2$ gas mixtures ($T_{gas}=1630$ K) this product reaches a maximum at H_2S additions of $x\sim 0.55\%$, as illustrated in Fig. 4a. Fig. 4b shows the way the calculated value of this product varies with

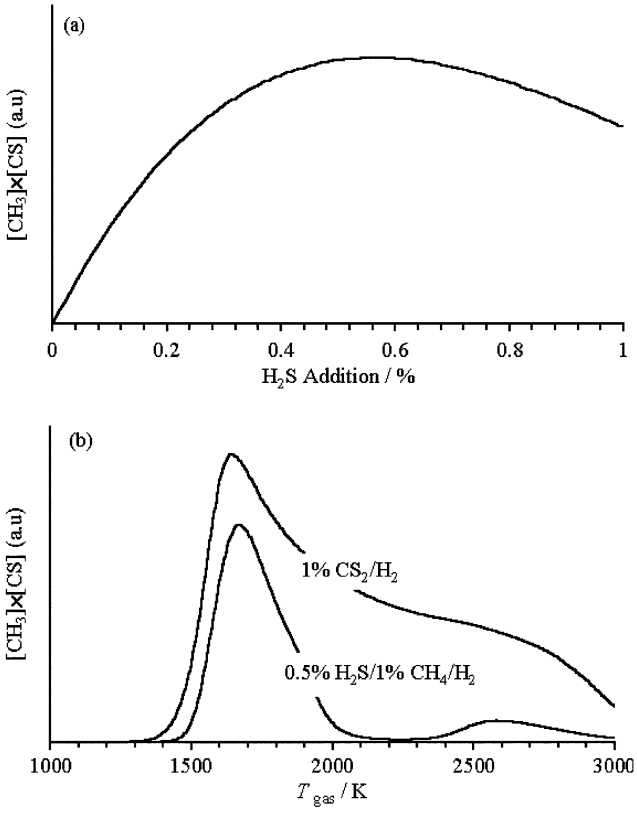

Fig. 4. Plots of the product $[CH_3]\times[CS]$ vs. (a) H_2S addition to $1\%CH_4/H_2$ gas mixtures ($T_{gas}=1630$ K) and (b) T_{gas} for $1\%CS_2/H_2$ and $0.5\%H_2S/1\%CH_4/H_2$ mixtures, as predicted by the SENKIN calculations. Conditions: pressure 20 Torr, reaction time $t=5$ s. The magnitude of the product $[CH_3]\times[CS]$ is proposed as providing a measure of the ability of a gas mixture to produce diamond films with high S-incorporation.

T_{gas}, for both 0.5%H_2S/1%CH_4/H_2 and 1%CS_2/H_2 gas mixtures. Both plots show maxima at $T_{gas} \sim 1600$ K—a value that must be similar to that used in previous attempts to obtain S-doped diamond [10,14,23]. That these were generally unsuccessful suggests that factors other than simply T_{gas} must determine whether H–C–S containing gas mixtures such as those studied here can be used to deposit S-doped diamond in which the S is incorporated into the diamond lattice in an electronically active state. One such factor might be the temperature gradient (and therefore, distance) from the HF or across the MW plasma sheath to the substrate surface, which could influence the transport and reaction of species produced in the hottest regions of gas (e.g. CH_3 and CS) as they diffuse towards the substrate. Perhaps, notable in this regard is the tendency for yellow sulfur to deposit on the cooler regions of the chamber walls [14], implying surface loss processes not included in the model. A potentially more important factor is the substrate temperature, as this will govern the various gas–surface reactions and any migration of surface species, thus influencing whether S incorporation might occur within the diamond lattice (either substitutionally or interstitially) or solely in the grain boundaries.

4. Conclusions

A mechanism has been proposed by which carbon and sulfur can couple in the gas phase diamond CVD environment to form CS and CS_2. This scheme is composed of several discrete reactions that can be summarised in the form of composite Reaction (1), which links CH_4, H_2S and CS_2. Arrhenius parameters have been assigned to each reaction step allowing, along with associated thermodynamic properties for each species, the mechanism to be used for SENKIN zero-dimensional computer simulations related to various H/C/S containing diamond CVD gas mixtures. The results of these calculations have been shown to be in good agreement with previous experimental measurements of MW (and to a lesser extent) HF activated CVD environments, thus validating the mechanism proposed previously [14]. It is also concluded that reactions neglected in this work (e.g. those occurring at the growing diamond surface) likely have greater influence on the degree and nature of S incorporation into polycrystalline CVD diamond films.

Acknowledgments

The authors are grateful to EPSRC for project funding, Element six for financial support (JRP) and Dr C.M. Western and E.J. Crichton for their many and varied contributions to aspects of this work.

References

[1] K.E. Spear, J.P. Dismukes, Synthetic Diamond-Emerging CVD Science and Technology, Wiley, New York, 1994.
[2] P.W. May, Philos. Trans. Roy. Soc. London, A 358 (2000) 473.
[3] B.V. Spitsyn, L.L. Bouilov, B.V. Derjaguin, J. Cryst. Growth 52 (1981) 219.
[4] K. Okano, Diamond: Electronic Properties and Applications, Kluwer Academic Publishers, Dordrecht, 1995.
[5] N. Vinocur, B. Miller, Y. Avyigal, R. Kalish, J. Electrochem. Soc. 143 (1996) L238.
[6] V.I. Polyakov, A.I. Rukovishnikov, N.M. Rossukanyi, A.I. Krikunov, V.G. Ralchenko, A.A. Smolin, et al., Diamond Relat. Mater. 7 (1998) 821.
[7] M. Hasegawa, D. Takeuchi, S. Yamanaka, M. Ogura, H. Watanabe, N. Kobayashi, et al., Jpn. J. Appl. Phys. 38 (1999) L1519.
[8] I. Sakaguchi, M.N. Gamo, Y. Kikuchi, E. Yasu, H. Haneda, Phys. Rev. B 60 (1999) R2139.
[9] M.N. Gamo, E. Yasu, C. Xiao, Y. Kikuchi, K. Ushizawa, I. Sakaguchi, et al., Diamond Relat. Mater. 9 (2000) 941.
[10] M.N. Gamo, C. Xiao, Y. Zhang, E. Yasu, Y. Kikuchi, I. Sakaguchi, et al., Thin Solid Films 382 (2001) 113.
[11] R. Kalish, A Reznik, C. Uzan-Saguy, C. Cytermann, Appl. Phys. Lett. 76 (2000) 757.
[12] S.C. Eaton, A.B. Anderson, J.C. Angus, Y.E. Evstefeeva, Y.V. Pleskov, Electrochem. Solid-State Lett. 5 (2002) G65.
[13] K. Nakazawa, M. Tachiki, H. Kawarada, Appl. Phys. Lett. 82 (2003) 2074.
[14] J.R. Petherbridge, P.W. May, G.M Fuge, G.F. Robertson, K.N. Rosser, M.N.R. Ashfold, J. Appl. Phys. 91 (2002) 3605.
[15] J.R. Petherbridge, P.W. May, G.M Fuge, K.N. Rosser, M.N.R. Ashfold, Diamond Relat. Mater. 11 (2002) 301.
[16] H. Sternschulte, M. Schreck, B. Strizker, Diamond Relat. Mater. 11 (2002) 296.
[17] C.A. Rego, R.S. Tsang, P.W. May, M.N.R. Ashfold, K.N. Rosser, J. Appl. Phys. 79 (1995) 7264, references therein.
[18] R.S. Tsang, P.W. May, M.N.R. Ashfold, K.N. Rosser, Diamond Relat. Mater. 7 (1998) 1651, references therein.
[19] S.M. Leeds, P.W. May, E. Bartlett, M.N.R. Ashfold, K.N. Rosser, Diamond Relat. Mater. 8 (1999) 1377.
[20] J.R. Petherbridge, P.W. May, S.R.J. Pearce, K.N. Rosser, M.N.R. Ashfold, J. Appl. Phys. 89 (2001) 1484, references therein.
[21] G.D. Barber, W.A. Yarbrough, J. Am. Ceram. Soc. 80 (1997) 1560.
[22] D.S. Dandy, Thin Solid Films 381 (2001) 1.
[23] R. Haubner, D. Sommer, Diamond Relat. Mater. 12 (2003) 298.
[24] J.R. Petherbridge, P.W. May, M.N.R. Ashfold, J. Appl. Phys. 89 (2001) 5219.
[25] R.J. Kee, F.M. Rupley, J.A. Miller, Sandia National Laboratories Report SAND89-8009B (1989).
[26] G.P. Smith, D.M. Golden, M. Frenklach, N.W. Moriarty, B. Eiteneer, M. Goldenberg, et al., http://www.me.berkeley.edu/gri_mech/.
[27] Gaussian 98, Revision A.7, M.J. Frisch, G.W. Trucks, H.B. Schlegel, G.E. Scuseria, M.A. Robb, J.R. Cheeseman, et al., Gaussian Inc., Pittsburgh PA, 1998.
[28] R.J. Kee, F.M. Rupley, J.A. Miller, Sandia National Laboratories Report SAND87-8215B (1994).
[29] M.N.R. Ashfold, P.W. May, J.R. Petherbridge, K.N. Rosser, J.A. Smith, Y.A. Mankelevich, N.V. Suetin, Phys. Chem. Chem. Phys. 3 (2001) 3471, references therein.

[30] A. Gicquel, K. Hassouni, Y. Breton, M. Chenevier, J.C. Cubertafon, Diamond Relat. Mater. 5 (1996) 366.
[31] D.G. Goodwin, J.E. Butler, in: M.A. Prelas, G. Popovici, L.K. Bigelow (Eds.), Handbook of Industrial Diamonds and Diamond Films, Marcel Dekker, New York, 1998, pp. 527–581, references therein.
[32] P. Roth, R. Lohr, U. Barner, Combust. Flame 45 (1982) 273.
[33] L.G.S. Shum, S.W. Benson, Int. J. Chem. Kinet. 17 (1985) 749.
[34] R. Humpfer, H. Oser, H. Grotheer, Int. J. Chem. Kinet. 27 (1995) 577.
[35] A. Amano, M. Yamada, K. Hashimoto, K. Sugiura, Nippon Kagaku Kaishi (1983) 385.
[36] W. Tsang, R.F. Hampson, J. Phys. Chem. Ref. Data 15 (1986) 1087.
[37] D.L. Baulch, C.J. Cobos, R.A. Cox, C. Esser, P. Frank, T. Just, et al., J. Phys. Chem. Ref. Data 21 (1992) 411.
[38] J.E. Nicholas, C.A. Amodio, M.J. Baker, J. Chem. Soc. Faraday Trans. 1 (75) (1979) 1868.
[39] K. Tsuchiya, K. Yamashita, A. Miyoshi, H. Matsui, J. Phys. Chem. 100 (1996) 17 202.
[40] D. Woiki, P. Roth, J. Phys. Chem. 98 (1994) 12 958.
[41] K. Scholfield, J. Phys. Chem. Ref. Data 2 (1973) 25.
[42] W.D. Good, J.L. Lacina, J.P. McCullough, J. Phys. Chem. 65 (1961) 2229.
[43] S.H.S. Wilson, M.N.R. Ashfold, R.N. Dixon, J. Chem. Phys. 101 (1994) 7538.
[44] B. Ruscic, J. Berkowitz, J. Chem. Phys. 98 (1993) 2568.